Obtaining spectral information from infrared scenarios using hyper-spectral cameras and cameras with spinning filter wheel

Eirik Glimsdal*, Erik Brendhagen, Jan Brede Thomassen,
Arthur D. van Rheenen, Lars Trygve Heen
Norwegian Defence Research Establishment (FFI), PO Box 25, N-2027 Kjeller, Norway

ABSTRACT

In the past decades the Norwegian Defence Research Establishment (FFI) has recorded and characterized infrared scenarios for several application purposes, such as infrared target and background modeling and simulation, model validation, atmospheric propagation, and image segmentation and target detection for civilian and defence purposes. During the last year FFI has acquired several new systems for characterization of infrared radiation properties. In total, five new infrared cameras from IRCAM GmbH, Germany, have been acquired. These cameras cover both the long-wavelength and extended medium-wavelength infrared spectral bands. The cameras are equipped with fast rotating filter wheels which can be used to study spectral properties and polarization effects within these wavelength bands. This option allows the sensors to operate in user-defined spectral bands. FFI has also acquired two HyperCam sensors from Telops Inc, Canada, covering the long-wavelength and extended medium-wavelength spectral bands, respectively. The combination of imaging detectors and Fourier Transform spectroscopy allows simultaneous spectral and spatial characterization of infrared scenarios. These sensors may optionally be operated as high-speed infrared cameras. A description of the new sensors and their capabilities are presented together with some examples of results acquired by the different sensors. In this paper we present a detailed comparison of images taken in different spectral bands, and also compare images taken with the two types of sensors. These examples demonstrate the principles of how the new spectral information can be used to separate certain targets from the background based on the spectral information.

Keywords: Infrared, infrared cameras, spectrometer, hyper-spectral imaging, long-wavelength, mid-wavelength.

1. INTRODUCTION

Using conventional infrared (IR) cameras, covering either the mid-wavelength (3-6 μm) or long-wavelength (8-12 μm) infrared band, typically only broad band images are acquired. The radiation from a source, after being transmitted through the atmosphere, is integrated over the spectral response of the camera to create the image. The camera signal is then proportional to the total radiation within this wavelength band. Two spectral sources with the same amount of radiation within the camera spectral response, but with different spectral properties, would give the same signal and appear equally bright in the recorded image. The two objects can therefore not be distinguished from each other based on the available information. Using either the measured spectral radiation curve, or isolating for instance two or more narrow bands, image segmentation and image processing based on this new available information can be used to gain more information about the scene than what can be obtained from just a pure broad band infrared image. Two spectrally different objects could then be distinguished from each other, for instance separating interesting targets from the background. This method is applicable both for solid materials and gas clouds, but generally gas clouds have stronger variations in spectral infrared radiation.[1]

2. MEASUREMENT EQUIPMENT

The measurement equipment used for the recordings presented in this paper consists of two HyperCam imaging spectrometers form Telops Inc., Canada [2], and two infrared cameras from IRCAM GmbH, Germany [3]. Both sets of sensors cover both the extended mid-wavelength (MWE) and long-wavelength (LW) infrared bands, respectively (see Table 1). The Telops HyperCam has standard optics with a 0.35 mrad instantaneous field of view (IFOV). The instrument can also be equipped with a 3.5x magnifying telescope giving a 0.10 mrad IFOV. Pictures of the instrument with and without the telescope are shown in Figure 1. The HyperCam has two integrated black-bodies (seen on each side of the centered aperture to the left in Figure 1) which are temperature controlled and are used as calibration sources.

*E-mail: eirik.glimsdal@ffi.no.

Electro-Optical Remote Sensing, Photonic Technologies, and Applications VIII; and Military Applications in Hyperspectral Imaging and High Spatial Resolution Sensing II, edited by Gary Kamerman, Gary J. Bishop, et al., Proc. of SPIE Vol. 9250, 92500M · © 2014 SPIE · CCC code: 0277-786X/14/$18 · doi: 10.1117/12.2066849

The two infrared cameras from IRCAM are standard infrared cameras covering the MWE- and LW-bands, respectively. Both cameras are equipped with fast rotating filter wheels running at up to 100 Hz frame rate. The filter wheel is positioned between the lens and the detector aperture, and can contain up to six different filters. An image sequence obtained from each filter position is therefore at maximum 16.7 Hz frame rate. The cameras are equipped with 50 mm, 100 mm and 200 mm lenses. For the measurements presented here the set of 200 mm lenses were used. The IR-cameras are shown in Figure 2, and some camera specifications are given in Table 1. The cameras also have a temperature controlled internal shutter which can be used for non-uniformity correction (NUC) of the image and for radiance calibration purposes.

Figure 1. Telops Inc. HyperCam. *Left:* Instrument with standard optics. *Right:* HyperCam with 3.5x telescope.

Figure 2. MWE and LW cameras from IRCAM GmbH with 200 mm lenses.

Table 1. Specifications for the MWE and LW IRCAM infrared cameras.

	IRCAM MWE camera	IRCAM LW camera	Telops MWE	Telops LW
Spectral band (FWHM)	1.5 - 5.6 µm	7.9 - 9.6 µm	1.5 - 5.5 µm	7.7 – 12.5 µm
Detector type	InSb	MCT	InSb	MCT
Detector array size	640 x 512	640 x 512	320 x 256	320 x 256
Pixel pitch	15 µm	24 µm	--	--
NETD	25 mK	30 mK	--	--
Frame rate	up to 100 Hz	up to 100 Hz	--	--
Interface	Gigabit Ethernet	Gigabit Ethernet	CameraLink	CameraLink
A/D output	14 bit	14 bit	16 bit	16 bit
Filter wheel	6 filter positions	6 filter positions	Single filter	Single filter
Available lenses	50, 100, 200 mm	50, 100, 200 mm	3.5x telescope	3.5x telescope
IFOV	0.075 mrad (FL 200)	0.12 mrad (FL 200)	0.1 / 0.35 mrad	0.1 / 0.35 mrad
FOV	2.7° x 2.2° (FL 200)	4.4° x 3.5° (FL 200)	1.8° x 1.5° / 6.4° x 5.1°	1.8° x 1.5° / 6.4° x 5.1°

3. EXPERIMENTS AND RESULTS

In this chapter some infrared images from recordings with the HyperCam sensors and with the IRCAM infrared cameras are presented and compared. We will concentrate on two examples, one scene where a gas plume is exhausted from the chimney of a central heating plant, and one scene showing a building with different wall materials. The results demonstrate the principles, and show examples, of how the spectral information can be used to separate certain areas and objects from the background, and examples of what kind of information which may be extracted from the images.

The recordings were obtained during two measurement periods, one in December 2013 and one in March 2014. During the first measurement period the scene contrasts were partly limited by the weather conditions. There was some fog, air temperature around 0 °C, high relative humidity and relatively low visibility. During the second measurement period the weather situation was much better. The sun was shining from a nearly clear blue sky for most of the time. The air temperature was around 5-10 °C, relative humidity was 60 %, and the visibility was good.

The MWE IRCAM camera was equipped with filters covering the following bands: (a) Open (pure substrate), covering the MW-camera spectral response; 1.5-5.6 µm [1800-6666 cm^{-1}], (b) 3.0-5.0 µm [2000-3333 cm^{-1}], (c) 4.35-4.60 µm [2170-2300 cm^{-1}] (covering most of the CO_2 emission lines in this spectral region), (d) 3.5-4.0 µm [2500-2860 cm^{-1}], (e) 3.3-3.5 µm [2820-3000 cm^{-1}], and (f) 2.1-2.3 µm [4420-4670 cm^{-1}]. All filters where on sapphire substrates and 1 mm thick (except filter (f) on 1 mm BK7 glass). No filters were inserted in the LW IRCAM camera.

Grayscales in the presented infrared images have been optimized to improve visibility, and are generally different in images presented side by side.

3.1 Plume from chimney

In this experiment, images of a chimney located a few hundred meters from the measurement location at Kjeller, Norway are recorded. The chimney emits exhaust gases and smoke from a central heating plant. The chimney was recorded during both periods, and the combustion was highest during the coldest weather conditions in December 2013. A wide field of view visual and a long-wavelength infrared image of the recorded scene in March 2014 are shown in Figure 3.

Figure 3. Visual image (*left*) and LWIR image (*right*) of a chimney on a central heating plant at Kjeller, Norway, recorded in March 2014. Field of view is not exactly the same in the two images.

3.1.1 Plume recordings with MWE infrared sensors in cold weather conditions

Close-up images of the chimney and plume recorded with the IRCAM MWE infrared camera in December 2013 are shown in Figure 4. The images are recorded with filter (a) to (d). Some differences between the four images may be pointed out: Not much difference is expected between filter (a) and (b) since the spectral bands both are quite broad. The main difference between the two is that filter (b) is not transmitting the wavelengths below 3 µm. The solar irradiation mostly influences the short wavelength part of the band, and this results in lower background signal from scattered solar radiation in filter (b) compared to (a), (only barely visible in image 4(a) and 4(b)). The contrast of the chimney itself therefore comes out slightly better in image 4(b). Filter (c) isolates most the signal from the strong CO_2 radiation from

the plume, while filter (d) is centered at shorter wavelengths outside this CO_2 band. The hot non-isolated top parts of the two inner pipes of the chimney are easily observed in image 4(d), while the plume is completely absent. We point out that if sufficient concentrations of soot or hot water droplets had been present in the plume, the plume might have been visible also in wavelength band (d). A metal rail on top of the chimney is heated by the warm exhaust gasses and visible in all MWIR images.

Images of the chimney recorded with the Telops MWE HyperCam at a different day in December 2013 are shown in Figure 5. Parts of the recorded spectrum are extracted and presented in each image. To increase the signal to noise ratio a number of individual datacubes[1] were averaged when the scene was recorded with the Telops instruments, resulting in a total recording time of several minutes. The images shown are therefore time-averages over the measurement time. This is contrary to the images in Figure 4, where the presented images are snap-shots from a recorded sequence. Image 5(i) shows the integrated 3-5 μm range, similar to what is obtained with camera filter (b) in Figure 4(b). Image 5(ii) shows an image integrated over a spectral band from 4.35 to 4.5 μm containing several of the spectral CO_2 emission lines. Image 5(iii) is composed from data points in a spectral band not containing CO and CO_2 emission lines (3.5 - 4 μm, similar to filter (d)). Image 5(iv) shows a difference image between image 5(ii) and 5(iii). We note that the plume and CO_2 emission from the two pipes inside the chimney becomes more distinguished in image 5(ii) compared to 5(i), as expected, and that the plume is almost absent in image 5(iii), where only the warm top of the chimney is visible (as in Figure 4(d)). The plume is then separated in image 5(iv), showing the difference between (ii) and (iii). The images presented in Figure 4 and 5 are recorded at different time and day and cannot be compared directly.

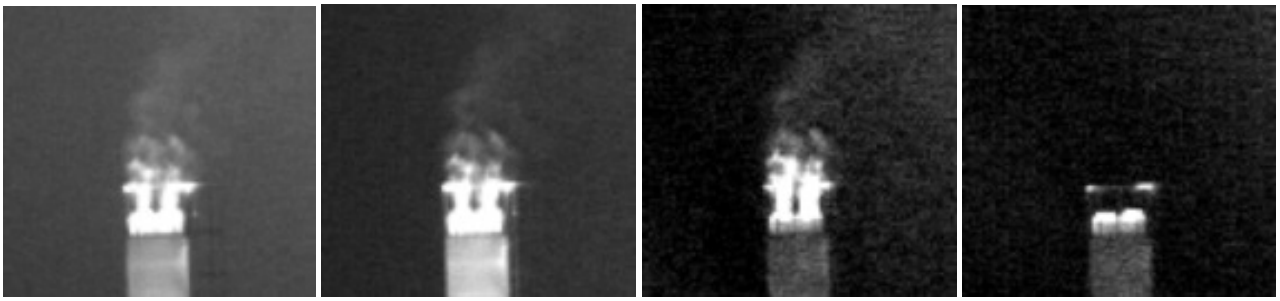

(a) (b) (c) (d)

Figure 4. Close-up images of the chimney and plume recorded with the IRCAM MWE IR camera in December 2013. The images are recorded with filters (a) to (d) from left to right.

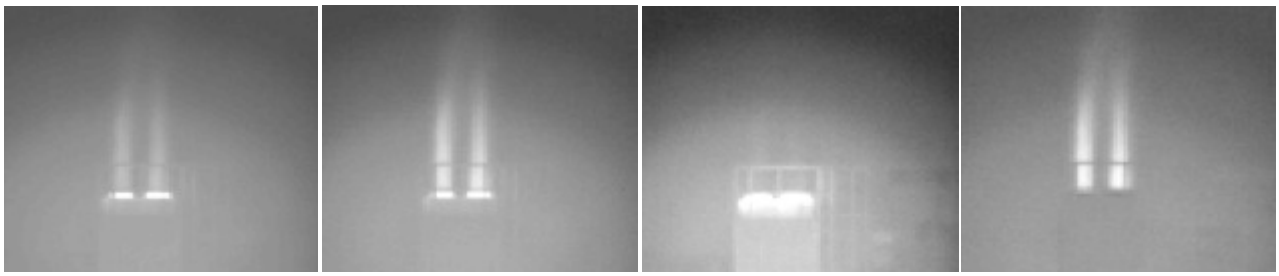

(i) (ii) (iii) (iv)

Figure 5. Close-up images of the chimney and plume recorded with the Telops MWE HyperCam sensor in December 2013. (i): Broad band 3-5 μm, (ii): wavenumbers with CO_2 emission lines, (iii): wavenumbers without CO_2 emission lines, (iv): difference (ii) - (iii).

The same image series as for the CO_2 emission in Figure 5 is shown for CO emission lines in Figure 6. The radiation from CO emission is much weaker than CO_2 in this case. Image 5(iii) is composed from data points in a spectral band not containing CO and CO_2 emission lines. Image 6(i) shows an image composed from spectral data points containing CO emission lines (just as image 5(ii) for CO_2). Image 6(ii) shows a difference image between image 6(i) and 5(iii), just as in Figure 5(iv). Image 6(i) indicates a difference in CO content between the two plumes arising from the two individual pipes inside the chimney. This becomes more prominent in the difference image in 6(ii), where CO emission

[1] A datacube is a three dimensional array containing a wavelength spectrum for each individual pixel in the image.

is found to mostly come from the right pipe only. This indicates a different combustion being responsible for this particular plume, compared to its left neighbor.

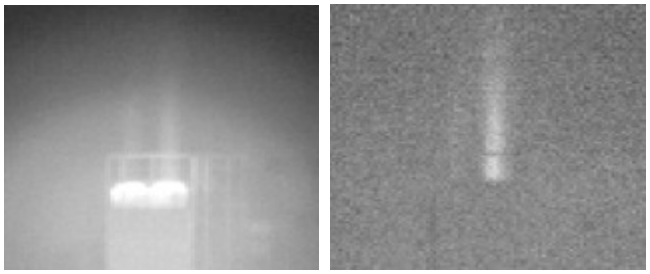

(i) (ii)

Figure 6. Close-up images of the chimney recorded with the Telops MWE HyperCam sensor in December 2014. (i): Wavenumbers with CO emission lines, (ii): Difference between 6(i) and 5(iii).

The spectrum from the left and right plume in Figure 5(i) is shown in Figure 7. The left diagram shows the spectral band from 4.55-4.65 μm, and the right diagram from 4.36 to 4.44 μm, covering some of the CO and CO_2 emission lines in this part of the spectrum, respectively. The left diagram shows the CO emission lines, which is found to be much stronger in the right plume, as also found in Figure 6(ii). The right diagram shows mostly CO_2 emission lines which are found to be quite similar in the two plumes, as also shown in Figure 5(iv). (The two curves are almost lying on top of each other).

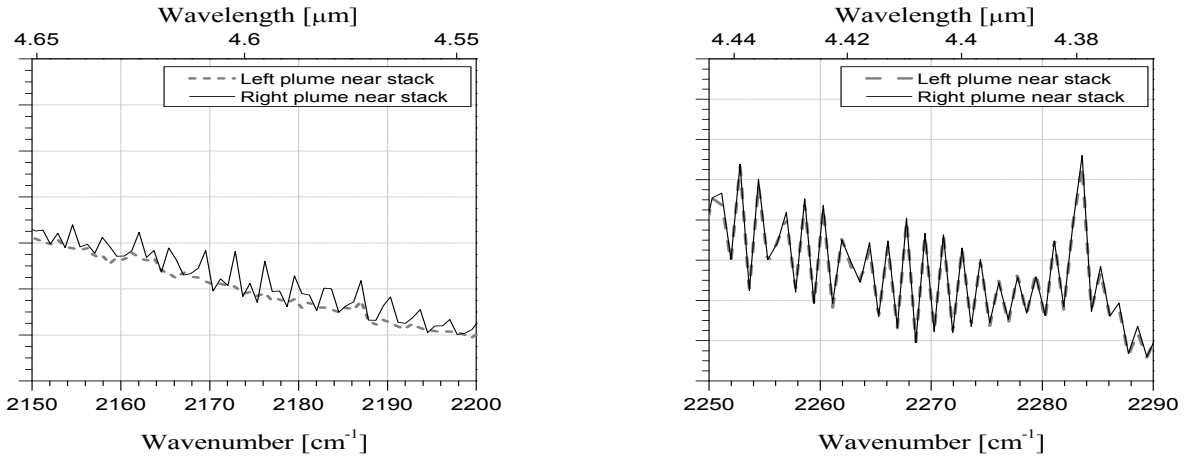

Figure 7. *Left*: Recorded spectrum of the left (dashed curve) and right (solid curve) plume from 4.55 to 4.65 μm, showing some of the CO-emission lines. *Right*: Recorded spectrum of the left and right plume from 4.36 to 4.44 μm, showing some of the CO_2-emission lines.

3.1.2 Plume recordings with LW infrared sensors in cold weather conditions

Comparing the LW IRCAM camera and Telops instrument, the IRCAM LW spectral response is narrower than for the HyperCam. More spectral data can then be obtained with the latter instrument. Images recorded with the LW HyperCam and LW IRCAM camera are shown in Figure 8 and 9, respectively. The same method as used to create the CO images in Figure 6 was used to create the image in Figure 8 showing CO_2 emission in the spectral band 9-10 μm. Figure 8(i) and (ii) show images composed from spectral data points with and without CO_2 emission lines, respectively. It is difficult to see any plume from the chimney in Figure 8(i), but it is possible to extract a low emission signal using the difference image in Figure 8(iii). No particular plume is observed in the LW IRCAM image to the left in Figure 9. The spectral response cut-off for this camera lies within the band with CO_2 emission lines, so the band is only partly covered by the camera. The CO_2 emission cannot be seen with this camera due to the combination of a single image from the camera, weak emission lines, a camera operating in a continuous spectral band and the spectral response. Note that the CO_2 emission in the LW is much lower than in the MW infrared band. The recorded plume spectrum with the HyperCam in the LW band from 9.1 to 10 μm is shown to the right in Figure 9.

(i) (ii) (iii)

Figure 8. Images of the chimney recorded with the Telops LW HyperCam sensor in December 2013. (i): Wavenumbers with CO_2 emission lines (see Figure 7), (ii): wavenumbers without CO_2 emission lines, (iii): difference (i) - (ii).

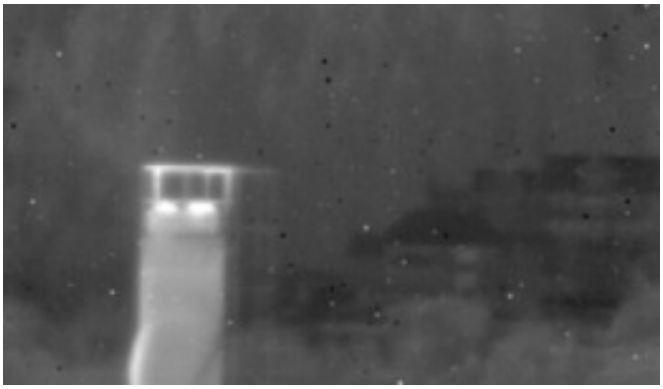

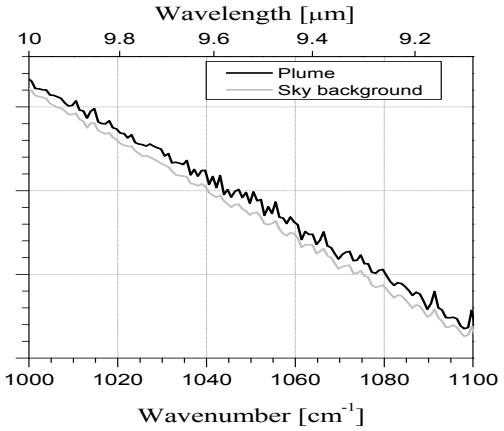

Figure 9. *Left*: LW infrared image of the chimney recorded with the LW IRCAM camera in December 2013. There are several uncorrected bad pixels in this image, which is seen as white or black individual pixels. *Right*: Recorded LW spectrum with the HyperCam of plume (black curve) and sky background (gray curve).

3.1.3 Plume recordings with MWE infrared sensors in warmer weather conditions

In March 2014 a new measurement series of the chimney was performed with both the Telops instruments and the IRCAM cameras. The weather was quite different this day than during the measurements in December 2013. Rather than cold, somewhat foggy weather with limited visibility, this day the weather was warm and clear. Recordings were made with the two sensor systems at the same time. Data from the two recording systems can then be compared directly. All six filter-positions were in use in the MWE IRCAM camera, with filters (a) to (f) as presented above. No filters were inserted in the LW IRCAM camera. Images recorded with each filter in the MWE IRCAM camera are shown in Figure 10. From the spectral/image hyper-data-cube recorded with the HyperCam the same spectral bands as filter (a) to (f) can be isolated and presented as images. This is shown in Figure 11. We can note that filter (f) is a relative narrow band pass filter, and as a result the noise level and image dynamics for this filter-position in Figure 10 is quite poor. Filter (e) is also quite narrow, which gives more noise in this image too, compared to the first four filters. (These challenges are discussed further in a later section.)

The HyperCam recordings presented in Figure 11 were obtained using the telescope mounted on the sensor. The presented images are based upon uncalibrated data, and a circular non-uniformity pattern arising from the telescope is present in the images. The image quality could have been improved by applying a telescope correction map or using large external blackbodies covering the telescope. Since the telescope is positioned in front of the two internal blackbody reference sources, using these sources to calibrate might give insufficient precision. Another reason for presenting uncalibrated results is that we did not measure any blackbody with sufficiently high temperature to produce a valid reference spectrum in the short-wave IR band during this experiment.

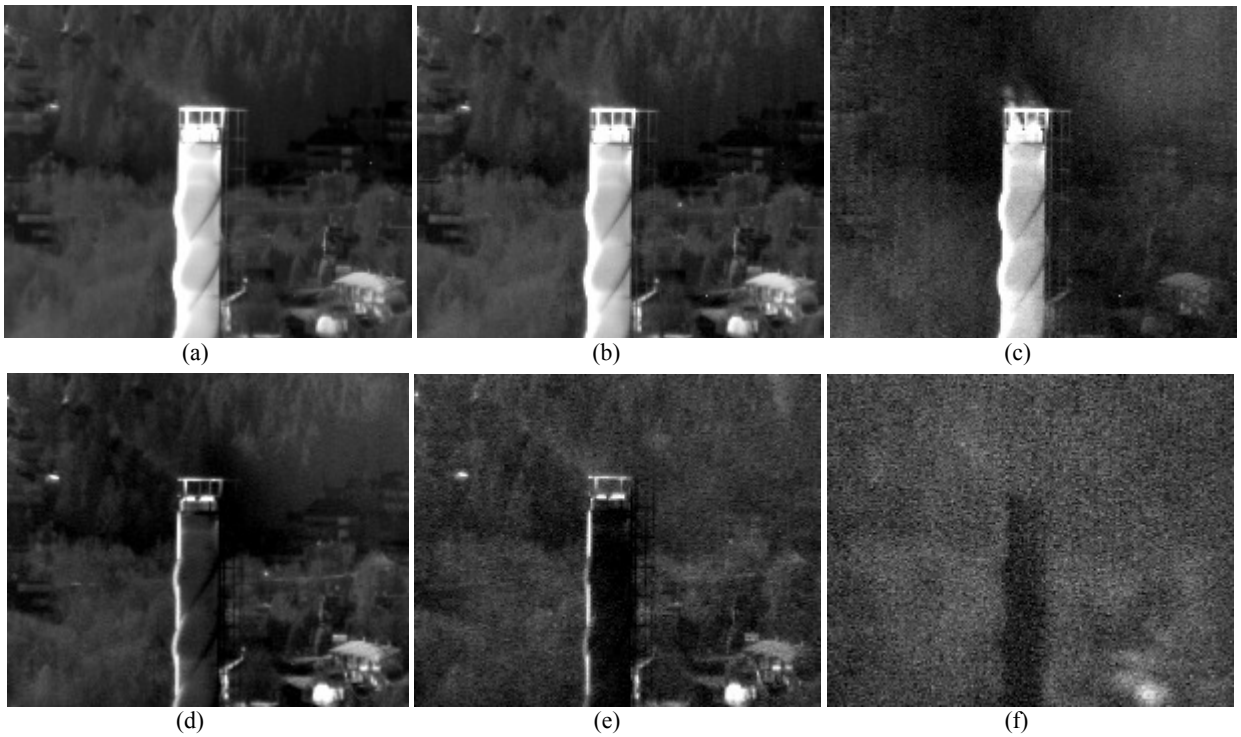

Figure 10. Images of the chimney recorded with the MWE IRCAM camera with spinning filter wheel in March 2014. Image number corresponds to the filter-name presented above: (a): Open; 1.5-5.6 μm, (b): 3.0-5.0 μm, (c): CO_2; 4.35-4.60 μm, (d): 3.5-4.0 μm, (e): 3.3-3.5 μm, and (f): 2.1-2.3 μm.

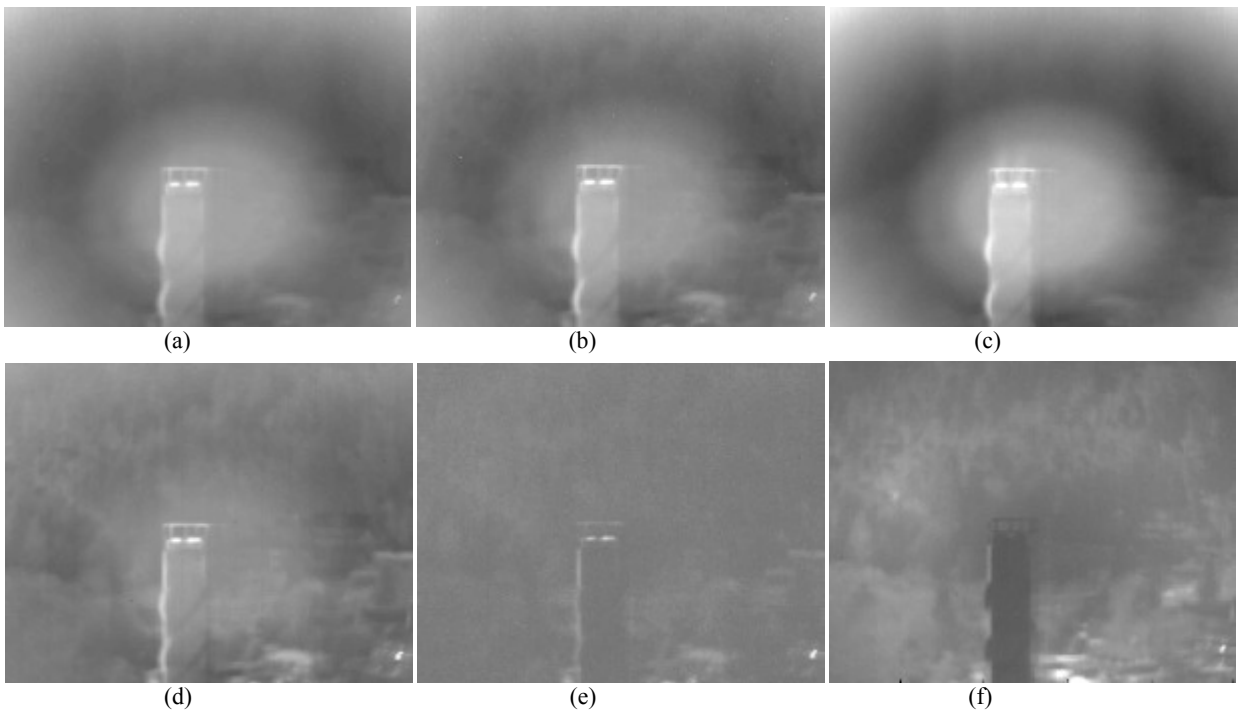

Figure 11. Images of the chimney recorded with the Telops MWE HyperCam sensor in March 2014. Image number corresponds to the filter-names presented above: (a): Open; 1.5-5.6 μm, (b): 3.0-5.0 μm, (c): CO_2; 4.35-4.60 μm, (d): 3.5-4.0 μm, (e): 3.3-3.5 μm, and (f): 2.1-2.3 μm.

We see that the plume is much weaker in Figure 10 and 11 than in Figure 4 and 5, due to lower activity in the heating plant on this day with higher outdoor temperature. Similar to Figure 4(c), it is possible to see that the plume is most prominent in Figure 10(c) and 11(c), where the CO_2 emission lines are strong. The plume is best visible between the top rails and the top of the pipes, where it is expected to have the highest temperature. The plume is present in images (a) and (b) also, but is difficult to see. The difference between images (a) and (b) is small. As for the previous measurement, the plume is almost absent in image (d), Figure 10(e) is quite similar to 10(d). Filter (f) is a short wavelength filter, and we see that the signal is dominated by solar scattering or radiation from the solar heated background. Since the shadow side of the chimney is observed it is not heated by the sun or having any direct solar reflections. The chimney then creates a negative contrast in this image. The same image features are found when comparing the two image series in Figure 10 and 11. The dataset is therefore found to be consistent comparing the two sensors.

3.2 Building with different wall materials and wall structures

In this experiment, a building vis-à-vis the FFI location at Kjeller, Norway is imaged in both the MWE and LW bands with the same two sets of sensors as for the chimney presented above. The building has four floors and the exterior paneling is made of different type of structured panels, and with different visual color. The walls next to, and between, the windows are flat surfaces colored blue. The walls above and below the windows are metallic surfaces with a grooved structure. The two upper floors are also built later than the two lower floors. The building has several windows some covered and some not covered with window blinds.

3.2.1 Recordings of the building with LW infrared sensors

A wide field of view visual and a long-wavelength infrared image of the recorded scene in March 2014 are shown in Figure 12. No filters were inserted in the LW IRCAM camera, so only a single image is recorded with this system in this wavelength band. The left side of the building is solar heated and under solar illumination during the measurements. The right side of the building is in the shade, and has been so for several hours. An image series of several isolated LW spectral bands recorded with the HyperCam is shown in Figure 13. The images are gray-scaled in order to get a good contrast between different areas on the shaded right side of the building. The window area on the left solar heated side is therefore white color saturated at the current chosen scaling (camera signal is not saturated).

Figure 12. Visual image (*left*) and LWIR image (*right*) of a building vis-à-vis the location of FFI at Kjeller, Norway. LWIR image recorded with the IRCAM camera showing parts of the second and third floor.

The blue colored panel on the solar heated side close to the corner (next to the windows with closed blinds) gives the strongest signal in the LWIR images in Figure 12 and 13. The solar heated window areas with open blinds also give a strong signal in the image, where the blinds and/or area inside are solar heated. The three closed blinds on the solar heated left side, seems much colder due to stronger reflections from the cold clear sky. There is also a notable difference between the signal from the plane surface (next to windows) and the grooved panels (above and below the windows), especially on the shaded side. The actual signal from an opaque surface is, as always, a combination of emitted and reflected radiation. Any difference in apparent temperature is then due to different surface emission and reflection properties. This might result in variations in surface temperatures also on the shadowed side, but these variations are believed to be small compared to the sun-illuminated side. From all images in Figure 13, we see that both the upper and lower grove panels on the shadowed side appear colder than the plane surface, meaning that it reflects more of the cold sky (diffuse reflections). In addition there is a large difference between the two groove panel areas above and below the

third floor windows. We note here that the third (and fourth) floor of this building is newer than the first two floors, and although the panels seem visually the same in Figure 12, the reflection properties are quite different.

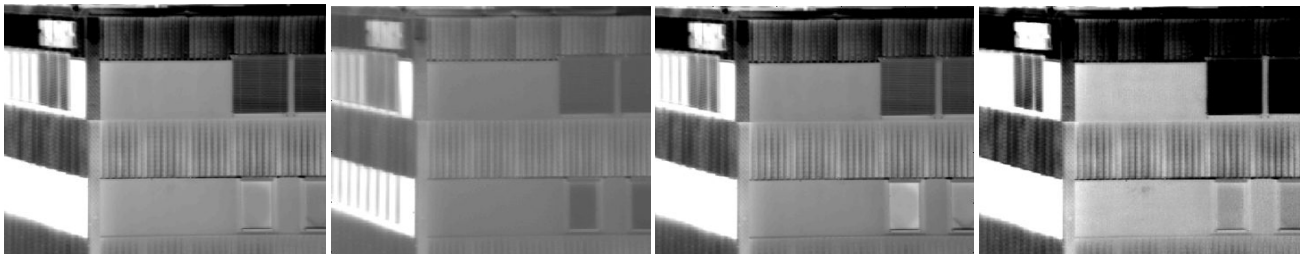

(i) (ii) (iii) (iv)

Figure 13. LWIR images of the building extracted from the LW HyperCam data-cube. (i): 7.7-11.7 μm [850-1300 cm^{-1}], (ii): 7.7-8.3 μm [1200-1300 cm^{-1}], (iii): 9.1-10.0 μm [1000-1100 cm^{-1}], (iv): 11.1-12.4 μm [805 - 900 cm^{-1}].

These observations are explained by the spectral curves to the left in Figure 14. The gray curve shows that the spectral radiance from the clear sky is high in spectral bands with low atmospheric transmittance, at low wavelengths around 8 μm and the band 9.4-10 μm, the latter mainly caused by radiation from the ozone layer. Between these bands and above 10 μm, where atmospheric transmittance is high, the spectral radiance is lower. The characteristics of the atmosphere is easily recognized in the spectral radiance from the upper groove wall (dashed curve), but only barely visible in the spectral radiance from the lower groove wall (black curve). The spectra show that the reflectivity of the upper groove wall is much higher than for the lower wall in the LWIR band. The result of this effect is that the upper groove wall appears colder in spectral bands where atmospheric radiance is low, while the lower part radiates more like a blackbody, thus giving much less variations in contrast between the blue wall and the lower groove surface.

For the selected bands shown in Figure 13, the effect is that the observed upper groove surface apparent temperature becomes lower as the wavelength increases. In the spectral band composing the image shown in Figure 13(ii), the sky radiance is quite high and thus the radiance from the upper and lower panels is quite similar. In Figure 13(iii) there is a mixture of high and low sky radiance which reflects off the upper panel and the radiance from this panel becomes lower than for the lower panel. The sky radiance is low in the band shown in Figure 13(iv), and the upper panel radiance is clearly lower than for the lower panel. The same variations in observed apparent temperatures between the different images in Figure 13 is also seen for the closed window blinds on the shaded building surface, because they typically have some reflection properties.

The calculated apparent temperatures in the LWIR image in Figure 12 are: Blue shaded surface: 18 °C, shaded grooved surface below windows: 15.5 °C, shaded grooved surface above windows: 11.5 °C, solar heated UNIK-logo above closed blinds: 22 °C, closed blinds: 16 °C, blue solar heated surface: 33 °C. All temperatures have variations of ±1-2 °C across the surface.

Looking at the window in the lower right corner of the image series in Figure 13, one sees a difference between the four images. In (i) (broad band image) the window seem to have low contrast with the blue plane surface around it. But, as the band is split up, we clearly see a negative contrast in both image (ii) and (iv), while a positive contrast is shown in (iii). Looking at the radiation spectrum obtained at this position compared to the blue wall surface in the right part of Figure 14, the radiation curves from these two surfaces are crossing at two points within this spectral band. This indicates spectral emissivity variations of one or both of the surfaces. The recorded spectrum explains the apparent colder window in Figure 13 (ii) and (iv), and the apparent warmer window in (iii).

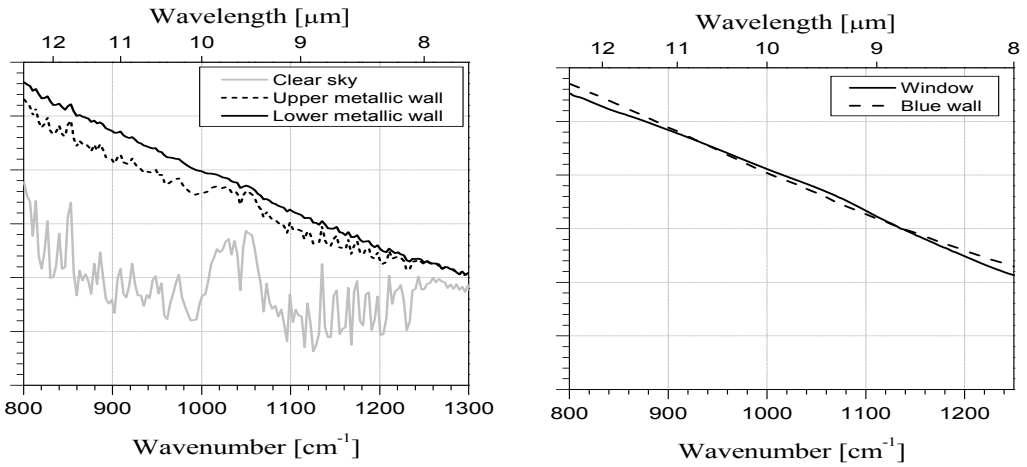

Figure 14. *Left*: Recorded LWIR spectrum with HyperCam sensor of the upper (dashed curve) and lower (solid black) groove metallic surfaces in Figure 13. Recorded radiation spectrum for the clear blue sky is shown for comparison (gray). *Right*: Recorded LWIR radiation spectrum with HyperCam for window (black curve) and blue wall (dashed) in Figure 13. Spectral resolution is 4 cm^{-1} in both figures.

3.2.2 Recordings of the building with MW infrared sensors

A series of recorded images with the MWE IRCAM camera with spinning filter wheel is shown in Figure 15. The filters are filter (a) to (f) as presented in the beginning of chapter 3. The sun-illuminated and shaded corner of the third floor is shown. A clear relative difference and change of contrast between the blue pained flat wall and the window blinds on the solar heated side is seen in the image series applying the different filters. The contrast between the plane surface and the window blinds was good in the broad LW infrared band presented above, while the contrast in the broad MWE band in Figure 15(a) is low. Applying filter (b) the contrast increases when only the 3-5 μm band is observed. This is explained by the fact that the high reflection of sun-light at short wavelengths now is being removed. This sun-light reflection in the closed blinds at low wavelengths is seen in Figure 15(f). This change is also found in the recorded spectrum, comparing the two surfaces in the different bands, as shown in Figure 17.

The contrast between the solar illuminated blue wall and window blinds surfaces is good in Figure 15(c) and low in (d) and (e). This correlates with the recorded spectra in Figure 17 (*left*) where the window blinds seem to reflect the cold sky well above 4 μm. The two presented spectra are similar in the 3-4 μm spectral band, and therefore the contrast is low in image (d) and (e) applying filters in this wavelength band. Images recorded with the HyperCam instrument, where data from the spectral bands corresponding to filter (a) to (f) is isolated, are shown in Figure 16. The images can be compared to the images in Figure 15, and it is found that the same features and contrast areas are present in both image series. We then conclude that the datasets from the two sensors are consistent.

A window (uncovered) on the shaded side of the building is seen in the lower right corner of the images in Figure 16. This is the same window that was discussed in the LW images in Figure 13 above. The MW image series displays negative, positive and low contrast for this window compared to the surrounding blue wall when the individual narrow bands are reviewed. The window has a clear negative contrast in the spectral band above 4 μm, low contrast between 3 μm and 4 μm, and a positive contrast below 3 μm, as correlates to the spectral data presented in Figure 18. (The spectral band between 2.5-3 μm is not shown and is not interesting due to dense atmospheric absorption here.) The positive contrast in the window at low wavelengths, may be a reflection of scattered radiation or a secondary reflection of a sun-illuminated surface.

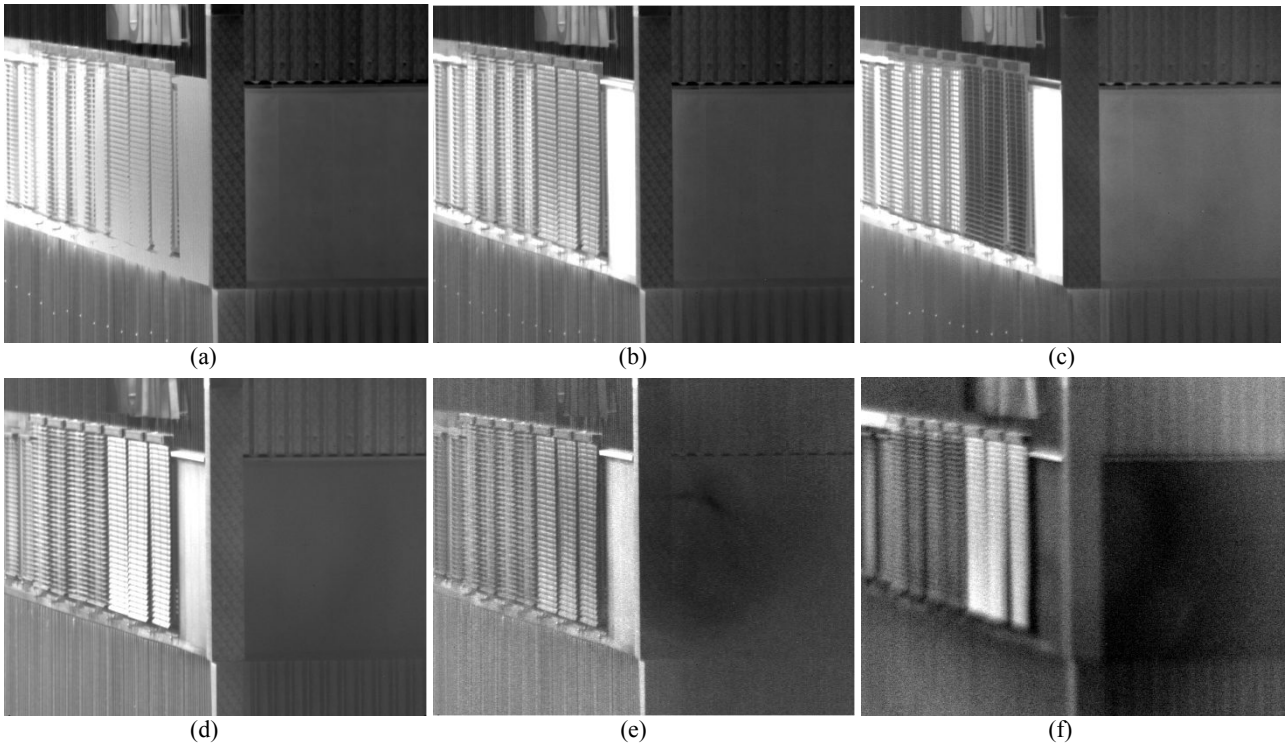

Figure 15. Images of the structured building recorded with the MWE IRCAM camera with spinning filter wheel in March 2014. Image number corresponds to the filter-name presented above: (a): Open; 1.5-5.6 µm, (b): 3.0-5.0 µm, (c): CO_2; 4.35-4.60 µm, (d): 3.5-4.0 µm, (e): 3.3-3.5 µm, and (f): 2.1-2.3 µm.

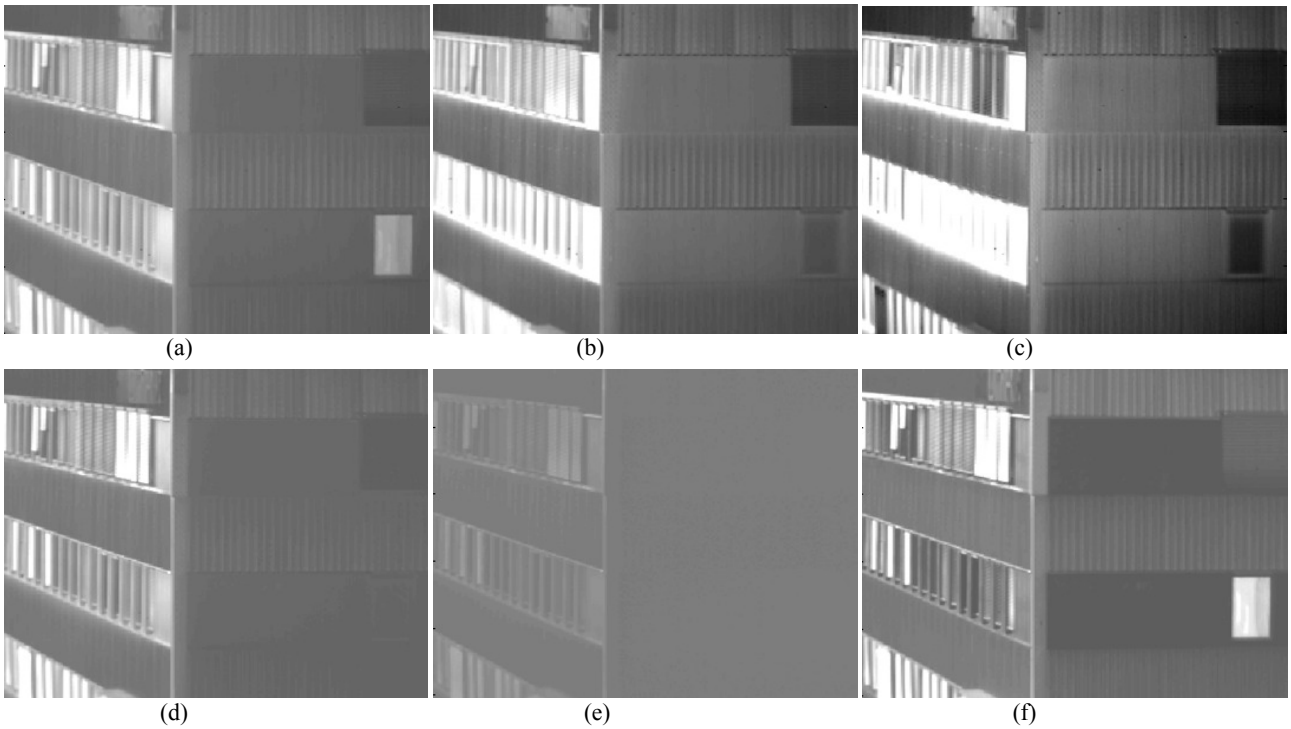

Figure 16. Images of the structured building recorded with the Telops MWE HyperCam sensor in March 2014. Image number corresponds to the chosen spectral bands corresponding to the filters presented above: (a): Open; 1.5-5.6 µm, (b): 3.0-5.0 µm, (c): CO_2; 4.35-4.60 µm, (d): 3.5-4.0 µm, (e): 3.3-3.5 µm, and (f): 2.1-2.3 µm.

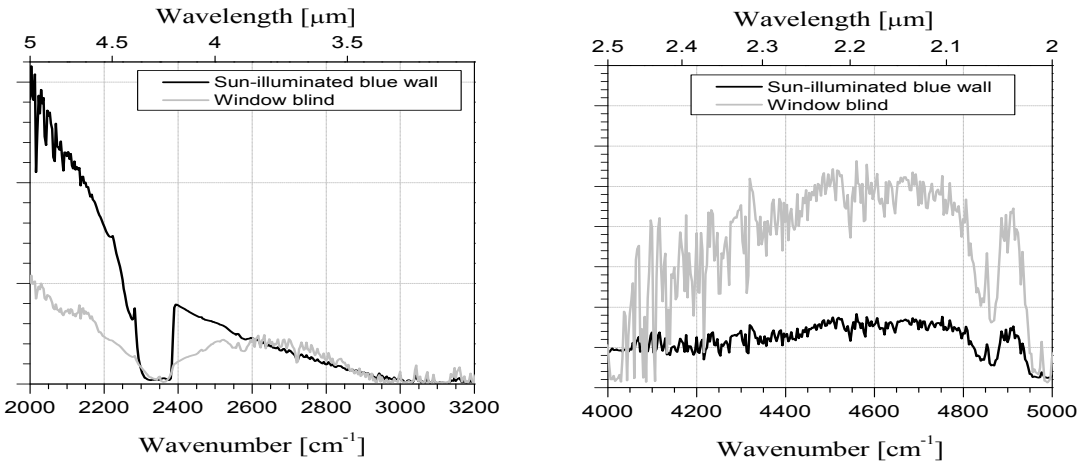

Figure 17. *Left*: Recorded MWIR spectrum with HyperCam sensor of the sun-illuminated blue wall (black curve) and window blind (gray curve) in Figure 15/16 for 3-5 μm wavelengths. *Right*: Recorded MWIR radiation spectrum for sun-illuminated blue wall (black) and window blind (gray) in Figure 15/16 for 2.0-2.5 μm wavelengths. Spectral resolution is 4 cm^{-1} in both figures.

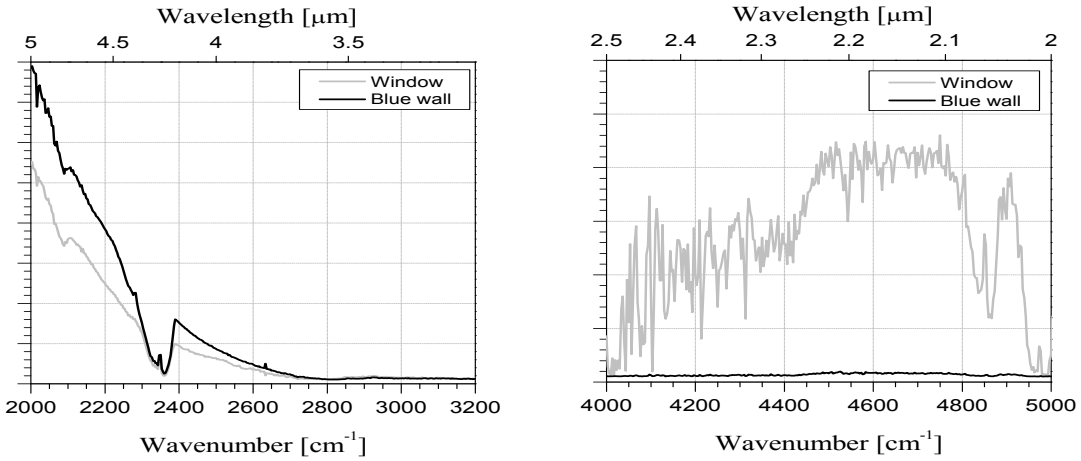

Figure 18. *Left*: Recorded MWIR spectrum with HyperCam sensor of the shaded blue wall (black curve) and window (gray) in Figure 16 for 3-5 μm wavelengths. *Right*: Recorded MWIR radiation spectrum for the shaded blue wall (black) and window (gray) in Figure 16 for 2.0-2.5 μm wavelengths. Spectral resolution is 4 cm^{-1} in both figures.

3.3 Comments on the results and challenges using the instruments

As all digital cameras, the IRCAM infrared cameras have a limited dynamic range. The integration time (analogue to the size of the aperture stop in a conventional camera) is changed in order to record a certain scene within the available dynamics, without being saturated. Decreasing the integration time will increase the noise, and increasing the integration time limits the dynamics. When applying narrow bandpass filters in the camera, one would like to increase the integration time in order to get more light onto the detector and thereby reduce noise. Using filters with different band pass width, the integration time must be set according to the most broad wavelength filter in order not to saturate this image at the highest intensity of radiation from the scene. The narrow band filters may then be quite noisy, as seen for instance in Figure 10(f). The dynamic range difference in the selected spectral bands thus is a performance limitation.

In order to get the same focus for all filters, the different filters must be of the same filter materials (refractive index) and thickness. More precisely, the filters need to have the same optical path length. Without this matching the focus will be different for each filter when the filter wheel is rotating, and it will be difficult to focus all images at the same time. This

effect results in image 15(f) being slightly out of focus using a 1 mm BK7 glass substrate here compared to 1 mm Sapphire for the other filters. At this short observation distance this small change in refractive index (1.5 vs. 1.7) is enough to change the focus, since the focus depth is short at these close-up distances.

Using the Telops HyperCam instrument, it is challenging to find the best balance between spectral resolution, frame size and data-cube rate. Increased spectral resolution and using a large frame size will increase the data-cube collection time significantly. The recording of one single data-cube can then take several seconds. Only static or quasi-static scenes can then be recorded with such settings. More dynamic scenes can be recorded by decreasing the spectral resolution and narrowing the frame size. The frame rate can then be increased to well above 1 Hz.

When using the telescope on the HyperCam, the calibration blackbody sources are located behind the telescope. Any non-uniformity pattern affecting the image coming from the telescope system are therefore difficult to remove by making non-uniformity recordings or other image calibration recordings with the internal blackbody sources. Large external blackbodies can be used to make calibration recordings in front of the detector, but the calibration process then becomes more complicated.

4. CONCLUSIONS

Some experiments with newly obtained infrared sensors at the Norwegian Defence Research Establishment (FFI) are presented. The instruments are two HyperCam sensors from Telops Inc., Canada, and two infrared cameras from IRCAM GmbH, Germany. Both pairs of sensors cover the extended mid-wavelength and long-wavelength infrared bands, respectively. The infrared cameras are equipped with spinning filter wheels, with six filter positions. Recording scenes in several sub-wavelength bands is then possible.

Images of two different infrared scenes are presented. The first scene is a chimney which emits exhaust gases and smoke from a central heating plant located at Kjeller, Norway. The recorded images from the different sub-wavelength bands show that the plume from the chimney appears different in the selected sub-wavelength bands. Emission lines from for instance CO and CO_2 can easily be distinguished and separated in the images.

The second scene is of a building with exterior paneling made of different types of structured panels, and with different visual color. The building also has several windows some covered and some not covered by window blinds. Different parts of the building create a good contrast with each other in some wavelength bands, and have low contrast with each other in other wavelength bands. The differences are explained through examination of the spectral image data. Using the information obtained from the spectral measurements can, in general, be of great importance when trying to separate certain particular areas/targets from for instance a background.

From the measurement series presented in this paper, a clear consistency between the obtained results from the IRCAM cameras compared to the HyperCam sensor is found. When splitting the hyper-cube data into the same wavelength bands as the filters mounted in the IRCAM camera, the same features found in the camera images are reproduced. It is also shown that general statements about the image results can be made based on the detailed spectral results obtained with the HyperCam sensors.

REFERENCES

[1] Brendhagen, Erik and Heen, Lars Trygve, “ShipIR model validation using spectral measurement results from the NATO SIMVEX trial”, Proceedings Targets and Backgrounds IX: Characterization and Representation, Vol. 5075, Orlando 2003.

[2] Telops Inc, Canada. www.telops.com, 2014

[3] IRCAM Gmbh, Germany. www.ircam.de, 2014